RSC Advances

PAPER

View Article Online
View Journal | View Issue

Cite this: *RSC Adv.*, 2020, **10**, 25059

Efficient blue electroluminescence with an external quantum efficiency of 9.20% and CIE_y < 0.08 without excimer emission†

Jayaraman Jayabharathi,* Sekar Sivaraj, Venugopal Thanikachalam and Balu Seransenguttuvan

Aromatically substituted phenanthroimidazoles at the C6 and C9 positions enhanced the thermal, photochemical and electroluminescence properties due to extension of conjugation. These new materials exhibit good photophysical properties with high thermal stability, good film-forming property and high luminous efficiency. The electroluminescence performances of C6 and C9 modified phenanthroimidazoles as host emitters were evaluated as well as the dopant in the fabricated devices. Among the non-doped devices, pyrene substituted PPI-Py or PPICN-Py based devices show maximum efficiency: PPI-Py/PPICN-Py: η_c (cd A^{-1}) – 9.20/9.98; η_p (lm W^{-1}) – 8.50/9.16; η_{ex} (%) – 5.56/5.80. The doped OLEDs, *m*-MTDATA/TAPC:PPI-Cz (4.81/4.85%), *m*-MTDATA/TAPC:PPICN-Cz (5.23/5.26%), *m*-MTDATA/TAPC:PPI-An (5.01/5.04%), *m*-MTDATA/TAPC:PPICN-An (5.25/5.28%), *m*-MTDATA/TAPC:PPI-Py (5.61/5.65%) and *m*-MTDATA/TAPC:PPICN-Py (5.76/5.78%) show improved device efficiencies compared to non-doped devices. Designing C6/C9 modified phenanthrimidazole fluorophores is an efficient strategy for constructing highly efficient OLEDs.

Received 18th April 2020
Accepted 26th June 2020

DOI: 10.1039/d0ra03463k

rsc.li/rsc-advances

1. Introduction

Efficient organic π-conjugated materials are very important in flat-panel displays due to their easy synthesis and tunable electrical properties with low power consumption[1–3] and energy source to sensitize the dopants for white emission.[4,5] The development of blue OLEDs lags behind compared to green and red counterparts due to the wider energy gap which leads to shorter operation lifetime, higher operation voltage and unbalanced charge injection/transportation, resulting in poor efficiency.[6–10] Restriction of π-conjugation length reduces the quantum yield and carrier transportation and leads to poor electroluminescence (EL) performance.[11,12] Therefore, systematic investigation of the structure–property relationship of blue emissive materials deserves consideration.[13–15]

Phenanthrimidazole (PI) with hole and electron transporting abilities is found to be an important building block for highly efficient NUV light emitting materials with high quantum yield.[16–26] Phenanthrimidazole with C2 substitution induced extension of conjugation and results in intramolecular charge transfer (ICT):[27–29] electron rich arylamine at C2 of 1,2-diphenyl-1*H*-phenanthro[9,10-*d*]imidazole leads to red-shifted UV emission to deep-blue emission,[27–29] however, N1 substitution does not promote significant photophysical change because of perpendicular configuration. The C2 and N1 substitution of phenanthrimidazole shifted far away from violet region.[30,31] To date, numerous reports have been published on phenanthrimidazole with C2 and N1 substitution, but substitution at C6 and C9 positions have not been widely studied.[32,33] Therefore, it is aimed to synthesise a series of different aromatically substituted (weak donors-N-phenylcarbazole, anthracene and pyrene) phenanthrimidazole (acceptor) at C6 and C9 positions to analyse luminous efficiency. Herein, we report series of blue emitters namely, 9-(8,9-dihydro-9-phenyl-4*H*-carbazol-3-yl)-1-(naphthalene-1-yl)-6-(9-phenyl-9*H*-carbazol-3-yl)-2-styryl-1*H*-phenanthro[9,10-*d*]imidazole (PPI-Cz), 4-(9-(8,9-dihydro-9-phenyl-4*H*-carbazol-3-yl)-6-(9-phenyl-9*H*-carbazol-3-yl)-2-styryl-1*H*-phenanthro[9,10-*d*]imidazole-1-yl)-naphthalene-1-carbonitrile (PPICN-Cz), (*E*)-6,9-bis(4,5-dihydropyren-2-yl)-1-(naphthalen-1-yl)-2-styryl-1*H*-phenanthro[9,10-*d*]imidazole (PPI-Py), (*E*)-4-(6,9-bis(4,5*a*1-dihydropyren-2-yl)-2-styryl-1*H*-phenanthro[9,10-*d*]-imidazol-1-yl)-1-naphthonitrile (PPICN-Py), (*E*)-6,9-di(anthracen-9-yl)-1-(naphthalen-1-yl)-2-styryl-1*H*-phenanthro[9,10-*d*]imidazole (PPI-An) and (*E*)-4-(6,9-di(anthracen-9-yl)-2-styryl-1*H*-phenanthro[9,10-*d*]imidazol-1-yl)-1-naphthonitrile (PPICN-An) and characterize them. Experimental results reveal that C6/C9 substitution provides moderate conjugated extension relative to C2 modification. The non-doped devices with pyrene substituted PPI-Py/PPICN-Py show maximum efficiency: η_c (cd A^{-1}) – 9.20/9.98; η_p (lm W^{-1}) – 8.50/9.16; η_{ex} (%) – 5.56/5.80. The doped OLEDs show improved device efficiencies with 20 wt%:

Department of Chemistry, Annamalai University, Annamalai Nagar, Tamilnadu – 608 002, India. E-mail: jtchalam2005@yahoo.co.in

† Electronic supplementary information (ESI) available. See DOI: 10.1039/d0ra03463k

m-MTDATA:PPI-Py/*m*-MTDATA:PPICN-Py: η_c – 8.56/9.13 cd A^{-1}; η_p – 8.23/8.87 lm W^{-1}; η_{ex} – 5.61/5.76%.

2. Experimental section

2.1. Materials and measurements

4,4′,4″-Tris(carbazol-9-yl)-triphenylamine (TCTA), 2,2′,2″-(1,3,5-benzinetriyl)-tris(1-phenyl-1*H*-benzimidazole) (TPBi) and *N*,*N*′-bis(naphthalen-1-yl)-*N*,*N*′-bis(phenyl)-benzidine (NPB) and other chemicals and solvents are purchased from Sigma-Aldrich. The H^1 and ^{13}C NMR spectra were recorded on Bruker 400 MHz spectrometer and mass spectra were recorded on Agilent LCMS VL SD. The UV-spectra was measured on Lambda 35 PerkinElmer (solution)/Lambda 35 spectrophotometer (RSA-PE-20) (film) instrument and emission spectra was recorded with PerkinElmer LS55 spectrometer. The quantum yield was calculated with fluorescence spectrometer Model-F7100 with integrating sphere. The decomposition temperature (T_d) and T_g (glass transition temperature) was measured with PerkinElmer thermal analysis system (10 °C min^{-1}; N_2 flow rate – 100 ml min^{-1}) and NETZSCH (DSC-204) (10 °C min^{-1}; N_2 atmosphere), respectively. Fluorescence lifetime was estimated by time correlated single-photon counting (TCSPC) method on Horiba Fluorocube-01-NL lifetime system: nano LED is excitation source with TBX-PS is detector; DAS6 software was employed to analyze the decay by reconvolution method. Oxidation potential of emissive materials were measured from potentiostat electrochemical analyzer (CHI 630A). Ferrocene was used as internal standard with HOMO of −4.80 eV and 0.1 M tetrabutylammonium perchlorate in CH_2Cl_2 as supporting electrolyte.

2.2. Computational details

The ground (S_0) (DFT)/excited (S_n^*) (TD-DFT) characteristics were examined by Gaussian 09 program[34] and multifunctional wavefunction analyzer (Multiwfn).[34]

2.3. Synthesis of emissive materials

2.3.1. 6,9-Dibromo-1-(naphthalene-1-yl)-2-styryl-1*H*-phenanthro[9,10-*d*]imidazole (DNSPI). A mixture of 3,6-dibromophenanthrene-9,10-dione (2.08 g, 10 mmol), cinnamaldehyde (1.51 g, 10 mmol), 1-naphthylamine (4.65 g, 50 mmol) with ammonium acetate (3.08 g, 40 mmol) in acetic acid (25 ml) was refluxed (120 °C; 12 h; N_2 stream) and poured into methanol. The separated pale yellow crude was purified by column chromatography on silica gel (petroleum ether : dichloromethane – 3 : 1) (Scheme S1†). Yield, 65.5%; ^1H NMR (400 MHz, $CDCl_3$): δ(ppm): 6.99 (s, 2H), 7.14–7.21 (m, 4H), 7.30–7.77 (m, 8H), 7.99–8.01 (t, 4H), 9.10 (d, 2H). ^{13}C NMR (100 MHz, $CDCl_3$): δ(ppm): 112.8, 120.9, 124.1, 125.7, 126.4, 127.8, 128.0, 128.3, 129.4, 130.5, 132.2, 133.4, 133.7, 134.6,135.2, 141.5.

2.3.2. 4-(6,9-Dibromo-2-styryl-1*H*-phenanthro[9,10-*d*]imidazole-1-yl)-naphthalene-1-carbonitrile (DSINC). A mixture of 3,6-dibromophenanthrene-9,10-dione (2.08 g, 10 mmol), cinnamaldehyde (1.51 g, 10 mmol), 4-aminonaphthalene-1-carbonitrile (4.65 g, 50 mmol) with ammonium acetate (3.08 g, 40 mmol) in acetic acid (25 ml) was refluxed (120 °C; 12 h; N_2 stream) and poured into methanol. The separated pale yellow crude was purified by column chromatography (petroleum ether : dichloromethane – 3 : 1) on silica gel (Scheme S1†). Yield, 75%; ^1H NMR (400 MHz, $CDCl_3$): δ(ppm): 6.70 (s, 2H), 6.92–7.30 (m, 4H), 7.40 (s, 1H), 7.50–7.80 (m, 4H), 7.85–7.98 (t, 4H), 8.20 (d, 2H), 9.00 (d, 2H). ^{13}C NMR (100 MHz, $CDCl_3$): δ(ppm): 108.3, 109.5, 111.1, 112.8, 115.8, 117.0, 118.1, 119.0, 120.1, 121.6, 122.2, 123.8, 125.2, 126.6, 127.5, 127.7, 127.8, 132.0, 132.7.

2.3.3. 9-(8,9-Dihydro-9-phenyl-4*H*-carbazol-3-yl)-1-(naphthalene-1-yl)-6-(9-phenyl-9*H*-carbazol-3-yl)-2-styryl-1*H*-phenanthro[9,10-*d*]imidazole (PPI-Cz). A solution of DNSPI (1.95 mmol), 9-phenyl-9*H*-carbazol-3-yl boronic acid (4.29 mmol), $Pd(PPh_3)_4$ (0.20 mmol) and aqueous Na_2CO_3 (2 M, 6 ml) in toluene (25 ml) and ethanol (10 ml) was refluxed (N_2 stream; 32 h). The solution was extracted with dichloromethane and the residue was purified by column chromatography (petroleum ether : dichloromethane – 2 : 1) to obtain white powder. Yield, 65.5%; ^1H NMR (400 MHz, $CDCl_3$): δ(ppm): 6.21 (s, 2H), 7.0–7.21 (m, 7H), 7.22–7.29 (m, 6H) 7.3–7.30 (m, 6H) 7.40–7.46 (m, 7H), 7.55 (d, 2H), 7.70 (d, 3H), 7.82 (s, 2H), 8.04 (d, 2H), 8.18 (t, 5H), 9.15 (s, 2H). ^{13}C NMR (100 MHz, $CDCl_3$): δ(ppm): 108.3, 111.1, 112.8, 117.0, 118.1, 119.0, 120.1, 121.6, 124.1, 125.2, 125.6, 126.3, 126.5, 127.8, 128.0, 128.3, 129.4, 130.7, 132.2, 133.0, 133.8, 135.2, 137.7, 141.1, 143.7, 144.3, 145.4. Anal. calcd $C_{69}H_{44}N_4$: C, 89.20; H, 4.77; N, 6.03. Found: C, 89.06; H, 4.28; N, 5.68. MS: *m*/*z*. 929.37 [M + 1]; calcd: 928.36.

2.3.4. 4-(9-(8,9-Dihydro-9-phenyl-4*H*-carbazol-3-yl)-6-(9-phenyl-9*H*-carbazol-3-yl)-2-styryl-1*H*-phenanthro[9,10-*d*]imidazole-1-yl)-naphthalene-1-carbonitrile (PPICN-Cz). The compound PPICN-Cz was prepared using the methodology similar to that of PPI-Cz by replacing DNSPI with DSPINC. Yield, 71%; ^1H NMR (400 MHz, $CDCl_3$): δ(ppm) 6.63 (s, 2H), 6.89–7.04 (m, 7H), 7.13–7.21 (m, 6H) 7.28–7.35 (m, 12H), 7.48–7.60 (m, 4H), 7.65–7.71 (m, 4H), 7.78 (d, 3H), 7.91–8.12 (t, 3H), 8.45 (s, 2H). ^{13}C NMR (100 MHz, $CDCl_3$): δ(ppm): 108.3, 109.5, 111.1, 112.8, 115.8, 117.0, 118.1, 119.0, 120.1, 121.6, 122.2, 123.8, 125.2, 126.6, 127.5, 127.7, 127.8, 132.0, 132.7. Anal. calcd $C_{70}H_{43}N_5$: C, 88.12; H, 4.54; N, 7.34. Found: C, 88.06; H, 4.26; N, 7.10. MS: *m*/*z*. 954.36 [M + 1]; calcd: 953.35.

2.3.5. (*E*)-1-(Naphthalen-1-yl)-9-(pyren-10-yl)-6-(pyren-2-yl)-2-styryl-1*H*-phenanthro[9,10-*d*]imidazole (PPI-Py). Yield, 71%; ^1H NMR (400 MHz, $CDCl_3$): δ(ppm): 6.78 (s, 2H), 7.14–7.21 (m, 3H), 7.30–7.51 (m, 6H), 7.60 (t, 6H), 7.71–7.79 (m, 9H) 7.82 (d, 2H), 8.0–8.40 (m, 2H), 8.18–8.22 (t, 6H), 9.15 (s, 2H). ^{13}C NMR (100 MHz, $CDCl_3$): δ(ppm): 112.8, 118.1, 123.0, 123.8, 124.9, 126.3, 126.5, 126.6, 127.2, 127.3, 127.8, 128.3, 128.7, 128.8, 129.5, 130.0, 130.7, 132.2, 134.6, 135.2, 137.7, 141.5. Anal. calcd $C_{65}H_{38}N_2$: C, 92.17; H, 4.52; N, 3.31. Found: C, 91.06; H, 4.06; N, 2.92. MS: *m*/*z*. 848.02 [M + 1]; calcd: 847.01.

2.3.6. (*E*)-4-(6,9-Di(dipyren-2-yl)-2-styryl-1*H*-phenanthro-[9,10-*d*]imidazol-1-yl)-napthalene-1-carbonitrile (PPICN-Py). Yield, 71%; ^1H NMR (400 MHz, $CDCl_3$): δ(ppm): 6.65 (s, 2H), 6.91–7.06 (m, 3H), 7.18 (d, 2H), 7.29 (d, 2H), 7.50–7.63 (m, 8H), 7.72 (s, 2H), 7.82–8.00 (m, 6H), 8.08–8.12 (t, 6H), 8.81 (s, 2H), ^{13}C NMR (100 MHz, $CDCl_3$): δ(ppm): 112.8, 118.1, 123.0, 123.8, 124.9, 126.3, 126.5, 126.6, 127.2, 127.3, 127.8, 128.3, 128.7, 128.8, 129.5, 130.0, 130.7, 132.2, 134.6, 135.2, 137.7, 141.5. Anal.

calcd $C_{66}H_{37}N_3$: C, 90.90; H, 4.28; N, 4.82. Found: C, 89.80; H, 4.26; N, 4.10. MS: *m*/*z*. 873.03 [M + 1]; calcd: 872.02.

2.3.7. (*E*)-6,9-Di(anthracen-9-yl)-1-(naphthalen-1-yl)-2-styryl-1*H*-phenanthro[9,10-*d*]imidazole (PPI-An). Yield, 71%; ^{1}H NMR (400 MHz, $CDCl_3$): δ(ppm): 6.82 (s, 2H), 7.14–7.20 (m, 4H), 7.30–7.34 (m, 6H) 7.40–7.62 (m, 12H), 7.70–7.84 (m, 6H), 8.04 (d, 2H), 8.15 (d, 2H), 9.21 (s, 2H). ^{13}C NMR (100 MHz, $CDCl_3$): δ(ppm): 112.8, 118.1, 124.1, 125.2, 126.3, 126.5, 126.6, 127.3, 127.6, 128.0, 128.7, 128.8, 130.3, 132.0, 132.2, 133.4, 134.6, 134.8, 137.7, 141.5. Anal. calcd $C_{61}H_{38}N_2$: C, 91.70; H, 4.79; N, 3.51. Found: C, 90.06; H, 4.26; N, 3.10. MS: *m*/*z*. 799.99 [M + 1]; calcd: 798.97.

2.3.8. (*E*)-4-(6,9-Di(anthracen-9-yl)-2-styryl-1*H*-phenanthro-[9,10-*d*]imidazol-1-yl)-1-naphthonitrile (PPICN-An). Yield: 71%; ^{1}H NMR (400 MHz, $CDCl_3$): δ(ppm): 6.71 (s, 2H), 6.85–7.10 (m, 3H), 7.21–7.28 (m, 6H), 7.31–7.48 (m, 6H), 7.50–7.60 (m, 6H), 7.74 (t, 5H), 7.92 (d, 2H), 8.03–8.15 (t, 3H), 8.75 (s, 2H). ^{13}C NMR (100 MHz, $CDCl_3$): δ(ppm): 109.5, 112.8, 115.8, 118.1, 121.7, 125.2, 126.3, 126.4, 127.3, 127.5, 127.6, 128.3, 128.5, 128.7, 130.3, 132.7, 135.2, 136.0, 137.7, 141.5. Anal. calcd $C_{62}H_{37}N_3$: C, 90.37; H, 4.53; N, 5.10. Found: C, 90.06; H, 4.26; N, 4.56. MS: *m*/*z*. 824.99 [M + 1]; calcd: 823.98.

2.4. Device fabrication and measurement

ITO glass (resistance 20 Ω sq^{-1}) was cleaned with acetone, deionized water and isopropanol, dried (120 °C) followed by UV-zone treatment (20 min) and transferred into deposition system. The devices were fabricated by multiple source beam deposition method in a vacuum at a pressure of 4×10^{-5} mbar. Evaporation rate of 2–4 Å s^{-1} (organic materials) and 0.1 and 4 Å s^{-1} for LiF and metal electrodes were applied, respectively. The thickness of each deposition layer was monitored with quartz crystal thickness monitor. The EL measurement with CIE coordinates was recorded with USB-650-VIS-NIR spectrometer (Ocean Optics, Inc, USA). The current density–voltage–luminance (J–V–L) characteristics were performed using source meter (Keithley 2450) equipped with LS-110 light intensity meter. The external quantum efficiency was determined from luminance, current density and EL spectrum assuming Lambertian distribution.

3. Results and discussion

The synthetic route for the emissive materials is displayed in Scheme S1:† efficient emitters namely, 9-(8,9-dihydro-9-phenyl-4*H*-carbazol-3-yl)-1-(naphthalene-1-yl)-6-(9-phenyl-9*H*-carbazol-3-yl)-2-styryl-1*H*-phenanthro[9,10-*d*]imidazole (PPI-Cz), 4-(9-(8,9-dihydro-9-phenyl-4*H*-carbazol-3-yl)-6-(9-phenyl-9*H*-carbazol-3-yl)-2-styryl-1*H*-phenanthro[9,10-*d*]imidazole-1-yl)-naphthalene-1-carbonitrile (PPICN-Cz), (*E*)-6,9-bis(4,5-dihydropyren-2-yl)-1-(naphthalen-1-yl)-2-styryl-1*H*-phenanthro[9,10-*d*]imidazole (PPI-Py), (*E*)-4-(6,9-bis(4,5*a*1-dihydropyren-2-yl)-2-styryl-1*H*-phenanthro[9,10-*d*]-imidazol-1-yl)-1-naphthonitrile (PPICN-Py), (*E*)-6,9-di(anthracen-9-yl)-1-(naphthalen-1-yl)-2-styryl-1*H*-phenanthro[9,10-*d*]imidazole (PPI-An) and (*E*)-4-(6,9-di(anthracen-9-yl)-2-styryl-1*H*-phenanthro[9,10-*d*]imidazol-1-yl)-1-naphthonitrile (PPICN-An) were synthesized by condensation followed by Suzuki-coupling reaction with appreciable yield and characterized by spectral techniques (Schemes S2–S5†).

3.1. Thermal and electrochemical properties

The twist angle between C6/C9 substituent and phenanthrimidazole plane in PPI-Cz, PPICN-Cz, PPI-Py, PPICN-Py, PPI-An and PPICN-An is about 55° which effectively suppress the conjugation and intermolecular π–π stacking. The twisted molecular architecture enhanced the thermal stability (T_d/T_g): PPI-Cz (492/213 °C), PPICN-Cz (502/215 °C), PPI-Py (550/261 °C), PPICN-Py (556/265 °C), PPI-An (490/180 °C) and PPICN-An (498/196 °C); high T_d reveal that these compounds would be capable of enduring vacuum thermal sublimation process. The high glass transition temperature (T_g) reveal that N-phenylcarbazole, pyrene and anthracene substituents at C6 and C9 positions enhanced their thermal and morphological stability, which are important for applications in organic electronic devices (Table 1 and Fig. 1). The relatively low T_d of anthracene compounds PPI-An/PPICN-An (490/492 °C) is attributed to steric hindrance which limits the conjugation. Among all compounds, pyrene derivatives (PPI-Py/PPICN-Py – 261/265 °C) show higher thermal stability and all these new born compounds exhibit higher T_d and T_g compared to C2-substituted Py-BPI (T_d/T_g – 431/137 °C).[35] These newly synthesized compounds show excellent thermal stability indicating that substitution at C6 and C9 position of phenanthrimidazole is a possible approach for enhancing thermal property. Such excellent thermal stability should be attributed to the incorporation of rigid pyrene, anthracene and N-phenylcarbazole unit at C6 and C9 position of bulky phenanthrimidazole. The higher thermal stability is beneficial for uniform amorphous film formation which is highly important for fabrication of devices.

The root-mean-square values (0.21 nm-PPI-Cz; 0.18 nm-PPICN-Cz, 0.23 nm-PPI-Py, 0.24 nm-PPICN-Py, 0.18 nm-PPI-An and 0.22 nm-PPICN-An) reveal absence of remarkable surface modification before and after annealing (30 °C : 90 °C; 12 h) which further supports the suitability of these materials for fabrication (Fig. S1a†). These compounds show reversible oxidation and reduction process implying that these materials are electrochemically stable and are bipolar carrier-transporting materials.

All these compounds show similar onset oxidation potentials but distinguishable CV curves due to different substituted aromatic rings.[36] The $E_{HOMO}[-(E_{onset} + 4.8)]$ eV/$E_{LUMO}[E_{HOMO} - 1239/\lambda_{onset}]$ have been calculated as: PPI-Cz (5.22/1.28 eV), PPICN-Cz (5.17/1.32 eV), PPI-An (5.05/1.46 eV), PPICN-An (5.00/1.58 eV), PPI-Py (4.96/2.04 eV) and PPICN-Py (4.92/2.16 eV). The HOMO energy of C6/C9 modified phenanthrimidazole derivatives are nearly same as that of TPI (~5.0 eV) which implies that the aromatic substitution at C6 and C9 positions would deepen LUMO level and leads to easier electron injection.

3.2. Molecular design

To gain a better insight into the electric properties of PPI-Cz, PPICN-Cz, PPI-Py, PPICN-Py, PPI-An and PPICN-An at molecular level, DFT calculation was performed. The HOMO of PPI-Cz

Table 1 Optical and thermal properties phenanthrimidazole derivatives

Properties	PPI-Cz	PPICN-Cz	PPI-An	PPICN-An	PPI-Py	PPICN-Py
λ_{abs} (nm) (soln/film)	252, 293, 330/256, 294	249, 286, 326/252, 288	313, 356, 370/331,373	308, 365/327, 370	342/354	340/351
λ_{em} (nm) (soln/film)	400, 416/410, 420	398, 406/406, 416	403/439	393/427	430/463	425/456
ϕ (soln/film) (%)	70/80/82	80/83/85	73/80/89	80/84/91	85/88/93	90/92/95
T_g/T_d (°C)	213/492	215/502	180/490	196/498	261/550	265/556
HOMO/LUMO/E_g (eV)	5.22/1.28/3.46	5.17/1.32/3.35	5.05/1.46/3.30	5.00/1.58/3.28	4.96/2.04/2.88	4.92/2.16/2.82
τ (ns)	6.2	6.0	5.5	5.0	3.5	3.1
$k_r \times 10^8$ (s^{-1})	0.11	0.13	0.13	0.16	0.24	0.29
$k_{nr} \times 10^8$ (s^{-1})	0.05	0.04	0.05	0.04	0.05	0.03

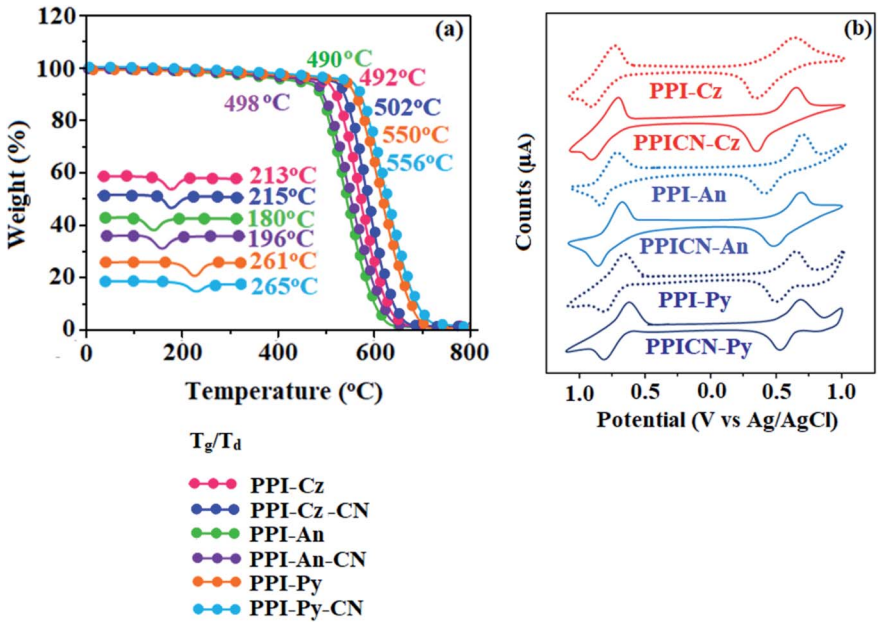

Fig. 1 (a) TGA and DSC; (b) cyclic voltammogram of emissive materials.

and PPICN-Cz populates on phenanthrimidazole core with partially on N-phenylcarbazole at C6/C9 except naphthyl fragment and the electron clouds in LUMO of PPI-Cz localized on C2 and N1 substituent with minor contribution on phenanthrimidazole core and LUMO of PPICN-Cz localized only on N1 substituent. The HOMO and LUMO of PPI-Py populates on C6 and C9 substituent, respectively whereas HOMO of PPICN-Py populates on both C6 and C9 substituents and LUMO mainly distributed on N1 substituent with partially on imidazole ring. The HOMO of PPICN-An populates on one phenyl of phenanthrimidazole core with partially on one phenyl of anthracene whereas the electron clouds in LUMO of PPICN-An localized mainly on C6 substituent (Fig. 2). Obviously, the HOMO and LUMO distribution implies that these materials are bipolar materials with charge transporting ability and become more efficient emitters in OLEDs.[37] The benzimidazole with C4 and C7 brominated molecule show dissimilar reactivity towards Suzuki coupling due to two different nitrogen atoms in imidazole ring leads to asymmetry in C4/C7 – modified benzimidazole derivative.[38] Similar trend was observed in C6/C7 substituted phenanthrimidazole derivatives. Tuning the substituent at C6/C9 positions make small influence on twist angles between phenanthrimidazole plane and naphthyl group and much larger variation in $\theta 3$ and $\theta 4$ angle (θ_1-PPI and C-coupling; θ_2-PPI and N-coupling; $\theta 3$-C6 and PPI; $\theta 4$-C9 and PPI-N-coupling). The synthesized emitters show more twisted configuration ($\theta_1 \sim 25°$; $\theta_2 \sim 75°$; $\theta_3 \sim 55°$; $\theta_4 \sim 56.0°$) due to larger steric hindrance between the substituent with phenanthrimidazole core (Fig. 2).

Phenanthrimidazole is an aromatic moiety with sextet of electrons in the conjugated system and the lone pair at N1 involved in the formation of conjugated system whereas the lone pair on N3 has no contribution. The conjugated lone pair can be transferred toward C6 or C9: electron migration toward C6 is more favourable since it results in largest charge separation (red arrow) than C9 (blue arrow) (Fig. S1b†). This preferred electronic structure leads to charge accumulation at C6 position and this unique electronic structure induced electron delocalisation on HOMO and LUMO at C6 and C9 substitutions, respectively and hence, this asymmetry enhanced the electron

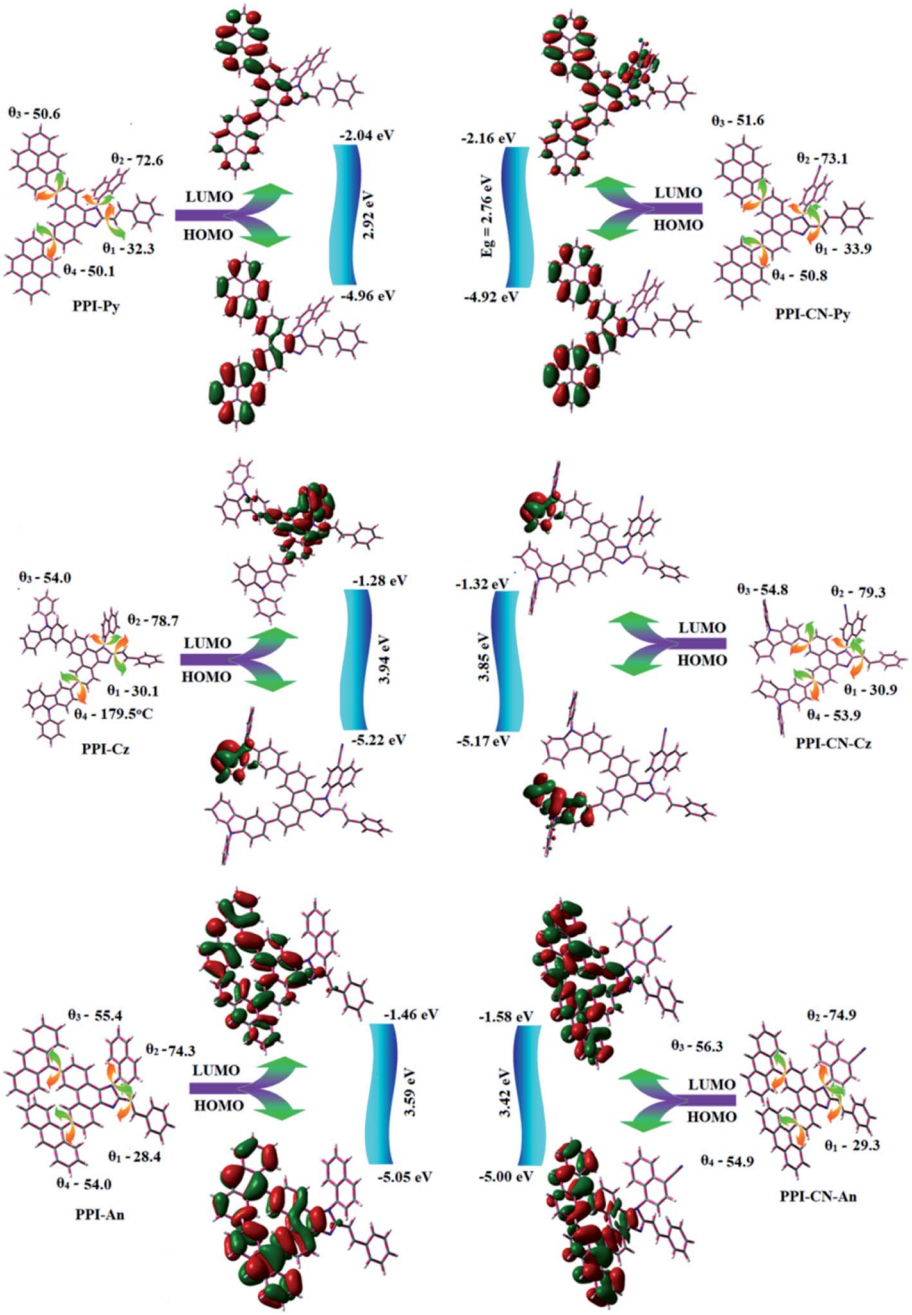

Fig. 2 Optimised geometry with dihedral angles and frontier molecular orbitals.

injection,[39] however, there is small overlap in HOMO and LUMO orbitals which endow the newborn emitters are efficient bipolar charge transporting materials leads to enhance the efficiency.

3.3. Photophysical properties

These new emitters show a weak absorption around ~249 nm attributed to π–π* transition of aryl ring in the imidazole core.[40–42] The strong absorption around ~286 nm and weak shoulder peak at longer wavelength (~326 nm) (Table 1 and Fig. 3) is assigned to π–π* transition of weak donor and phenanthrimidazole fragments and charge transfer transitions, respectively.[43] The absorption of the synthesized compounds is red-shifted relative to parent due to the highly conjugated anthracene/pyrene/N-phenylcarbazole with phenanthrimidazole core. Anthracene substituted phenanthroimidazoles PPI-An/PPICN-An show characteristic anthracene absorption bands 313, 356, 370/308, 365 nm. The pyrene substituted PPI-Py/PPICN-Py show vibronic broad absorption at 342/340 nm with high intensity which supports the charge transfer electronic interactions. Furthermore, red-shifted absorption implies the conjugation of N-phenylcarbazole, anthracene and pyrene with phenanthrimidazole core. The film absorption spectra of PPI-Cz, PPICN-Cz, PPI-Py, PPICN-Py, PPI-An and PPICN-An is comparable to those of solution. The optical energy

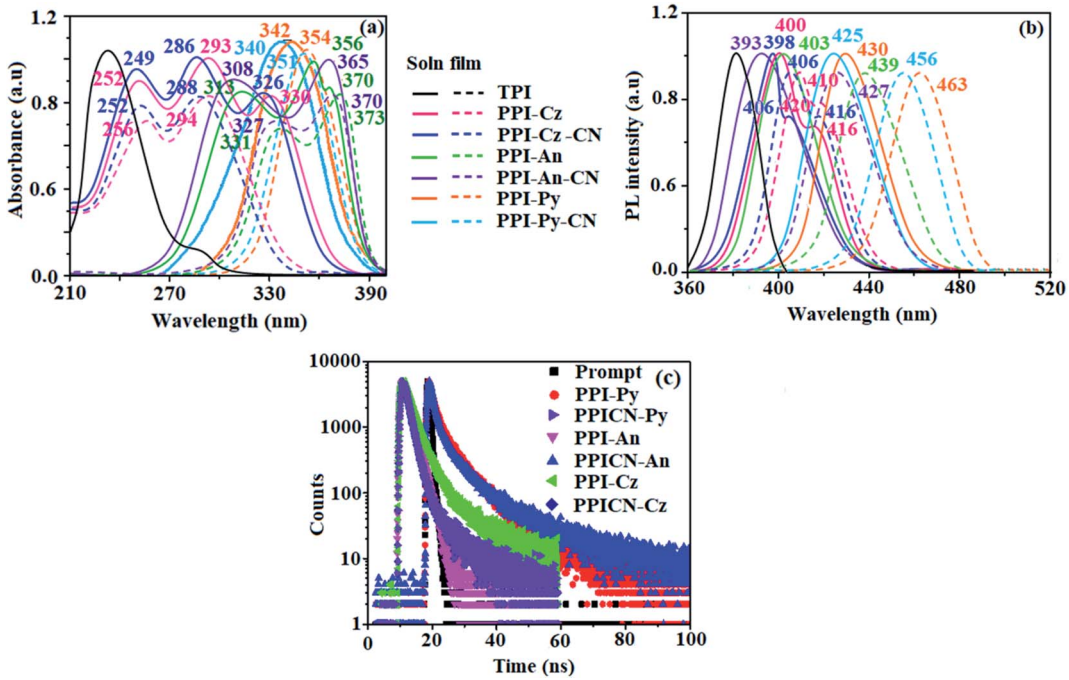

Fig. 3 (a) Normalized absorption; (b) emission and (c) decay curve of emissive materials.

gap (E_g) of 3.14, 3.11, 2.95, 2.92 2.90 and 2.88 eV for PPI-Cz, PPICN-Cz, PPI-An, PPICN-An, PPI-Py and PPICN-Py, respectively calculated from absorption onset. Although one more pyrene ring is incorporated to phenanthrimidazole moiety in PPI-Py or PPICN-Py, its absorption does not significantly red-shifted and comparable E_g to that of 1-(4-*tert*-butylphenyl)-2-(4-(pyren-1-yl)phenyl)-1*H*-phenanthro[9,10-*d*]imidazole (Py-BPI). Also these compounds show intense absorption with higher molar extinction coefficient (ε) of 2.9×10^5 M^{-1} cm^{-1} (PPI-Py) and 3.0×10^5 M^{-1} cm^{-1} (PPICN-Py). Similar trend was observed for other emitters: 3.4×10^5 M^{-1} cm^{-1} (PPI-Cz), 3.5×10^5 M^{-1} cm^{-1} (PPICN-Cz) or 2.8×10^5 M^{-1} cm^{-1} (PPI-An), 2.7×10^5 M^{-1} cm^{-1} (PPICN-An) or PPI-Py or PPICN-Py. The effect of C6 and C9 modification on emission follows variation as shown in absorption spectra (Fig. 3).

The PL spectra of PPI-Cz (400 nm), PPICN-Cz (398 nm), PPI-An (403 nm), PPICN-An (393 nm), PPI-Py (430 nm) and PPICN-Py (425 nm) show strong violet emission and weak shoulder peak at 416 nm (PPI-Cz) and 406 nm (PPICN-Cz). The PL spectra of solid film PPI-Cz (410, 420 nm), PPICN-Cz (406, 416 nm), PPI-AN (439 nm), PPICN-An (427 nm), PPI-Py (463 nm) and PPICN-Py (456 nm) is also in violet region. The film of PPI-Cz, PPICN-Cz, PPI-An, PPICN-An, PPI-Py and PPICN-Py show wide bathochromically shifted emission relative to solution (Fig. 3). The PL spectrum of solid thin film of PPI-Cz and PPICN-Cz, is located in the NUV region, with only ~14 nm (PPI-Cz) and ~10 nm (PPICN-Cz) red shifts, in which peak at 410 nm (PPI-Cz) and 406 nm (PPICN-Cz) is weak with respect to that in solution and the high intensity peak at 420 nm (PPI-Cz) and 416 nm (PPICN-Cz) become the main emission peak due to the polarization effect existed in the solid state. The emissive spectra of the fluorophore can be tuned from violet-blue to deep-blue region through modification of TPI with N-phenylcarbazole, anthracene and pyrene. These new compounds show narrow FWHM of around ~45 nm which is similar to that of isolated

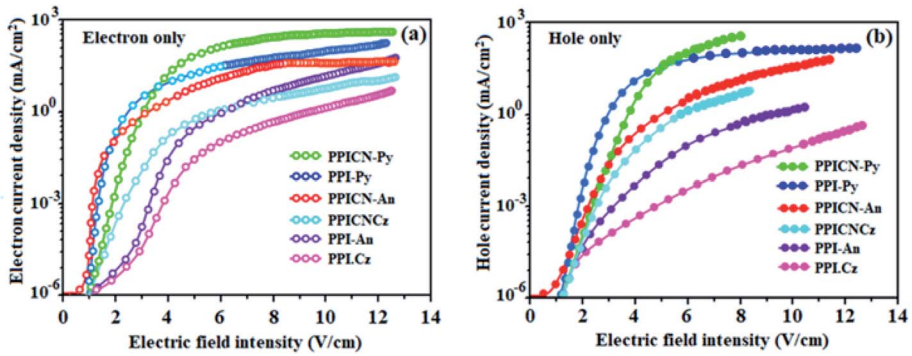

Fig. 4 (a) Hole-only and; (b) electron-only devices of emissive materials.

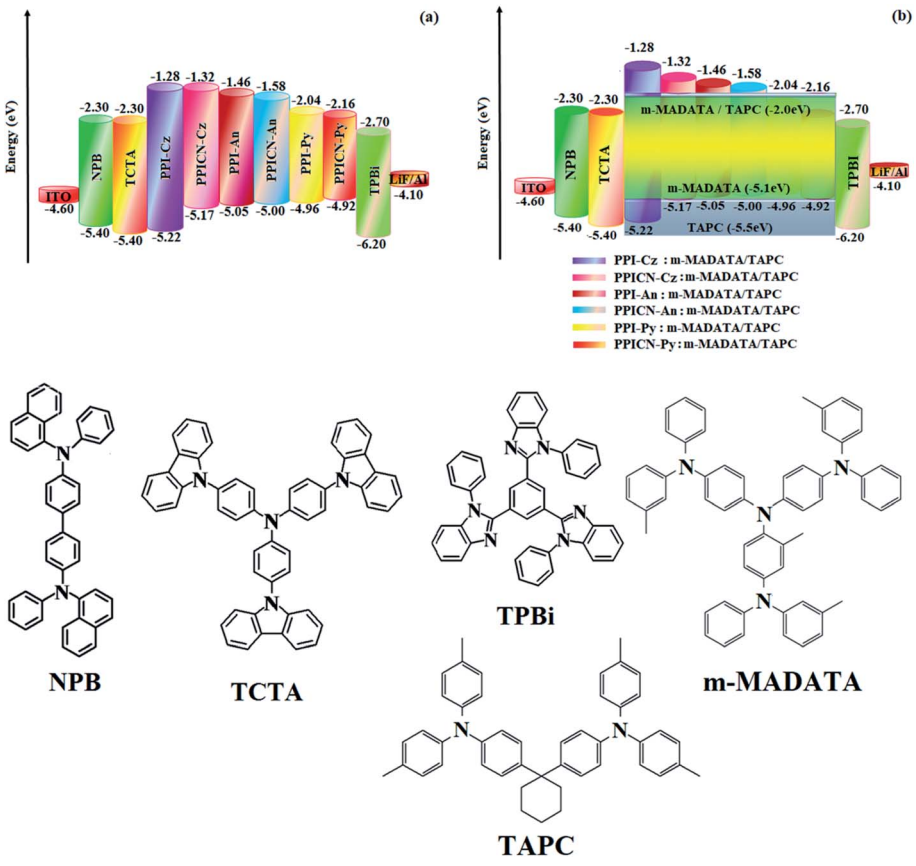

Fig. 5 Energy level diagram of non doped (a) and doped devices (b).

phenanthrimidazole (51 nm) and it is different from C2- and N1-substituted phenanthrimidazole derivatives.[44,45] These derivatives show broaden emission peak with larger red shift in film. The film of anthracene based PPI-An and PPICN-An emitters exhibit broad emission with long tail in longer wavelength region mainly due to intermolecular stacking induced by peripheral anthracene groups. All these materials emit prompt fluorescence with lifetime shorter than 10 ns. The fluorescence lifetime of C6/C9 substituted compounds are comparable to that of parent indicating that C6/C9 modification does not affect fluorescence decay significantly (Table 1 and Fig. 3). The new born blue emitters show high quantum yield (solution/film) of PPI-Cz (0.70/0.80), PPICN-Cz (0.80/0.83), PPI-An (0.73/0.80), PPICN-An (0.80/0.84), PPI-Py (0.85/0.88) and PPICN-Py (0.90/0.92). The C6 and C9 modification show improved photoluminescence quantum yield (PLQY) in film to assess the substitution effect on photophysical properties: pyrene substituted PPI-Py (0.85/0.88) and PPICN-Py (0.90/0.92) has taken as a model C6, C9- substituted derivative compared to C2-modified Py-BPI molecule.[46]

To further investigate the excited state properties, solvent effect on photophysical properties was studied (Fig. S2 and S3†). The PPI-Cz, PPICN-Cz, PPI-An, PPICN-An, PPI-Py and PPICN-Py show red shifted emission with gradually widened and structureless profile along with increasing orientation polarization of the medium due to intramolecular charge transfer electronic interaction in the excited states.[47] The photophysical properties are also in agreement with DFT calculation, both experimental and theoretical results imply that phenanthrimidazole group serve as central emitting core as well as an ICT inducer. The ICT behaviour of phenanthroimidazoles was studied by solvatochromic studies (Tables S1–S6†). Interaction between solvent and dipole moment of solute can be described by Lippert–Mataga model.[47] $hc(\hat{\upsilon}_{abs} - \hat{\upsilon}_{flu}) = hc(hc\hat{\upsilon}^{vac}_{abs} - hc\hat{\upsilon}^{vac}_{flu}) + 2(\mu_e - \mu_g)^2/a_o^3\ [(\varepsilon - 1/2\varepsilon + 1) - 1\backslash 2(n^2 - 1/2n^2 + 1)]$ [μ_g and μ_e – ground state and excited state dipole moment, $\hat{\upsilon}_{abs}$ and $\hat{\upsilon}^{vac}_{abs}$ – solvent-equilibrated absorption maxima (λ_{abs}) and extrapolated to gas phase, $\hat{\upsilon}_{flu}$ and $\hat{\upsilon}^{vac}_{flu}$ – solvent equilibrated fluorescence maxima (λ_{emi}) and extrapolated to gas-phase, respectively, a_o – Onsager cavity and ε and n-solvent dielectric constant and refractive index, respectively].

The linear variation of Stokes shift with $f(\varepsilon,n)$ has been shown in Fig. S4† where double linear correlation is obtained. Polar protic solvents fall on a separate line indicating that the mode of solvation of the emitting state is different from that in polar aprotic solvents. For polar protic solvents, the gradual increment of stokes shift is due to intermolecular hydrogen bonding interactions. Although small μ_e is obtained in solvents with low Δf (<0.17) 10.11 D-PPI-Cz; 12.98 D-PPICN-Cz; 10.87 D-PPI-An, 13.46 D-PPICN-An; 11.08 D-PPI-Py; 13.88 D-PPICN-Py; high μ_e of 20.11 D-PPI-Cz; 26.87 D-PPICN-Cz; 22.31 D-PPI-An, 26.12 D-PPICN-An; 22.48 D-PPI-Py; 26.92 D-PPICN-Py is

obtained in high Δf (>0.17). This ICT property is expected to enhance the EL performances of these compounds.[48–52] These studied compounds exhibit overall increase of Stokes shift from non-polar to polar aprotic solvents mainly due to the combined effect of increasing polarity of the medium and intramolecular charge transfer state. The charge transfer properties of all emissive materials were supported theoretically (Fig. S5–S11 and Tables S7–S15†).

3.4. Electroluminescence properties

N-phenylcarbazole, anthracene and pyrene substituted phenanthroimidazoles are expected to have good electron transport properties irrespective of aromatic substituents and also close packing in the solid state which is supported by optical properties. These compounds show good hole conductivity due to excellent hole transport property of phenanthrimidazole moiety.[53]

Single-carrier devices were fabricated to confirm the electrical properties: (a) ITO/NPB (10 nm)/PPI-Cz or PPICN-Cz or PPI-An or PPICN-An or PPI-Py or PPICN-Py (60 nm)/NPB (10 nm)/LiF (1 nm)/Al (100 nm) (hole-only device): (b) ITO/TPBi (10 nm)/PPI-Cz or PPICN-Cz or PPI-An or PPICN-An or PPI-Py or PPICN-Py (60 nm)/TPBi (10 nm)/LiF (1 nm)/Al (100 nm) (electron-only device). Fig. 4 shows the current density *versus* voltage characteristics of hole-only and electron-only devices and reveal that these materials have better electron injection and transport properties. The difference in current density between hole-only and electron-only devices is negligible, suggesting that these materials are potential bipolar materials capable of transporting electrons and holes in devices.[54–56]

3.5. Electroluminescence performances

The non-doped OLEDs with configuration of ITO/NPB (60 nm)/TCTA (25 nm)/PPI-Cz or PPICN-Cz or PPI-An or PPICN-An or PPI-

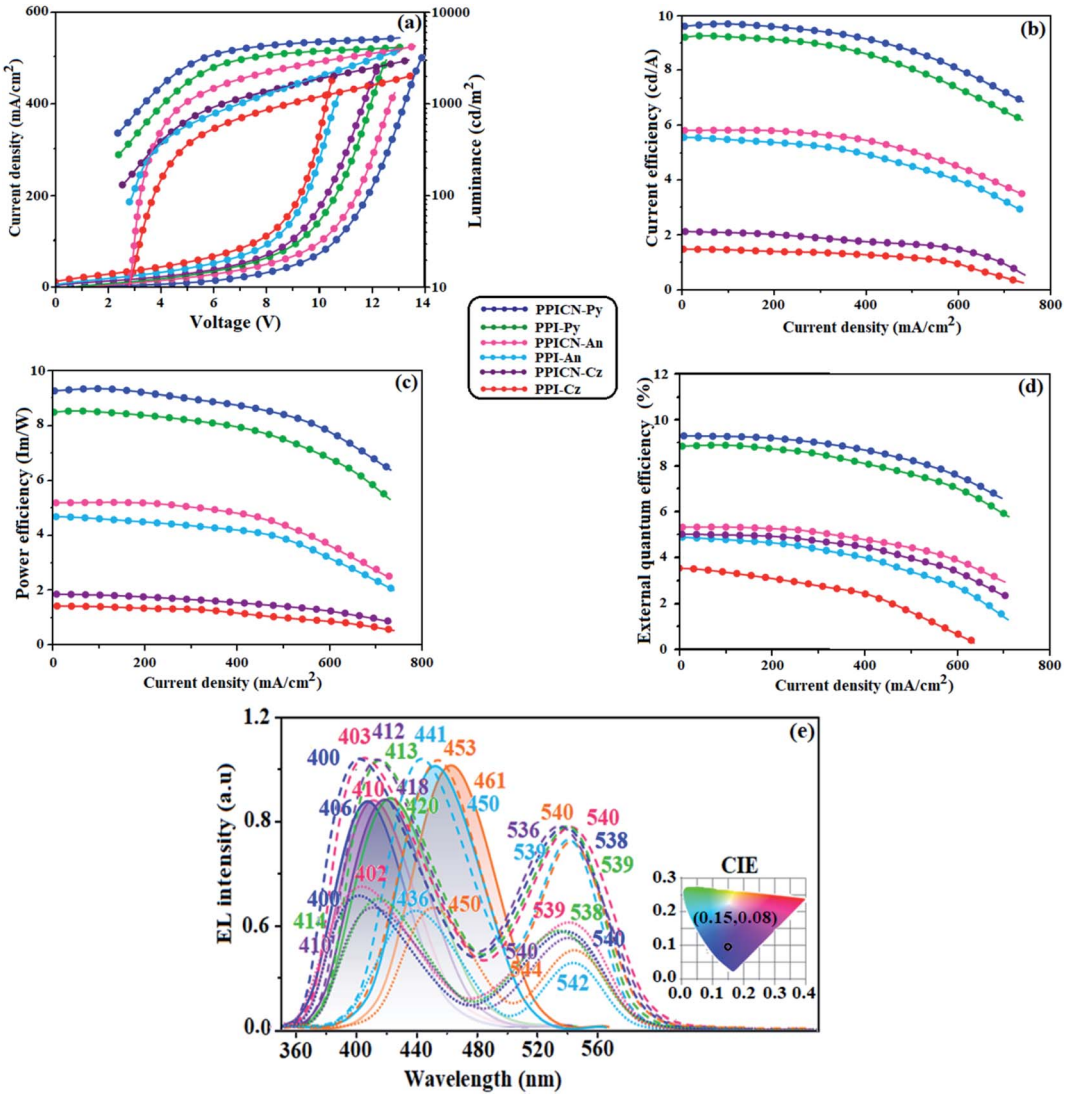

Fig. 6 Non-doped device efficiencies: (a) luminance/current density–voltage; (b) current efficiency–current density; (c) power efficiency–current density; (d) external quantum efficiency–current density; (e) EL spectra of emissive materials (inset: CIE) of emissive materials.

Table 2 Electroluminescent performances of non-doped devices

Properties	PPI-Cz	PPICN-Cz	PPI-An	PPICN-An	PPI-Py	PPICN-Py
V_{on} (V)	2.6	2.5	2.6	2.6	2.4	2.4
η_c (cd A^{-1})	1.40	2.10	5.89	5.98	9.20	9.98
η_p (lm W^{-1})	1.32	1.98	4.62	5.03	8.50	9.16
η_{ex} (%)	3.56	5.02	4.08	5.10	5.56	5.80
EL (nm)	410	406	420	418	461	450
CIE (x,y)	0.15, 0.06	0.15, 0.05	0.15, 0.06	0.20, 0.06	0.15, 0.08	0.15, 0.08
L (cd m^{-2})	2956	3168	3805	4186	4016	4546

Py or PPICN-Py (30 nm)/TPBi (25 nm)/LiF (1 nm)/Al (100 nm) have been fabricated (Fig. 5): NPB (*N*,*N*′-di-1-naphthyl-*N*,*N*′-diphenylbenzidine) and 1,3,5-tris(*N*-phenylbenzimidazol-2-yl)-benzene (TPBi) have been functioned as electron- and hole-blocking materials, respectively. 4,4′,4″-tris[3-methylphenyl(phenyl)amino]triphenylamine (*m*-MTDATA) was employed as hole-transporting as well as electron-blocking layers.

The low turn-on voltage of the nondoped devices using PPI-Cz (2.6 V), PPICN-Cz (2.5 V), PPI-An (2.6 V), PPICN-An (2.6 V), PPI-Py (2.4 V) and PPICN-Py (2.6 V) is because of good charge transportation and small E_g of emitters (Table 1). A low energy barrier among the devices promotes the charge injection. The formed exciton is well confined within the emissive layer due to large energy gap of TCTA and TPBi. The TPBi layer block the hole because of shallow HOMO energy (−6.3 eV). The non-doped devices exhibit linear current density-luminance characteristics and show typical photoelectric characteristics (Fig. 6).

Current density of the fabricated devices increased steeply with increase of voltage due to smaller energy gap and shallow LUMO energy. The non-doped devices show maximum efficiency: PPI-Cz/PPICN-Cz: η_c (cd A^{-1}) – 1.40/2.10; η_p (lm W^{-1}) – 1.32/1.98; η_{ex} (%) – 3.56/5.02, PPI-An/PPICN-An: η_c (cd A^{-1}) – 5.89/5.98; η_p (lm W^{-1}) – 4.62/5.03; η_{ex} (%) – 4.08/5.10 and PPI-Py/PPICN-Py: η_c (cd A^{-1}) – 9.20/9.98; η_p (lm W^{-1}) – 8.50/9.16; η_{ex} (%) – 5.56/5.80 (Table 2 and Fig. 6). Among all the emitters, pyrene substituted PPI-Py and PPICN-Py shows excellent efficiencies at low driving voltage due to small injection barrier. The energy level diagram shown that the hole injection barrier at TCTA:PPI-Py (0.34 eV) and TCTA:PPICN-Py (0.38 eV) junction and electron injection barrier at TPBI:PPI-Py (0.66 eV) and TPBI:PPICN-Py (0.54 eV) junction is negligible. Such suitable energy levels and small injection barrier would promote both balanced hole and electron balanced injection and transportation leads to enhanced efficiency.[57] The PPI-Py/PPICN-Py based non-doped device emission of 461/450 nm with CIE of (0.15, 0.08). The PPI-Cz/PPICN-Cz based devices show stable near ultra-violet emission at 410/406 nm with CIE coordinates of (0.15, 0.06/0.15, 0.05) and no excimer or exciplex peak can be observed implying that hole and electron recombination is well confined within the emissive layer.[58] The OLED using PPI-An/PPICN-An shows greenish blue emission 420/418 nm (CIE: 0.15, 0.06). The hypochromatic shift in the EL spectra (Fig. 6) compared to the PL spectra is probably due to weak microcavity effects.[59–64]

The non-doped devices based on PPI-Cz, PPICN-Cz, PPI-An, PPICN-An, PPI-Py and PPICN-Py show stable blue emission with CIE (0.15, 0.06), (0.15, 0.05), (0.15, 0.06), (0.15, 0.06), (0.15, 0.08) and (0.15, 0.08), respectively. To further improve the efficiency and colour purity, we have used PPI-Cz, PPICN-Cz, PPI-An, PPICN-An, PPI-Py and PPICN-Py as emissive dopants and 4′,4″-tris[3-methylphenyl(phenyl)amino]triphenylamine (*m*-MTDATA) and 1,1-bis((di-4-tolylamino)phenyl)cyclohexane (TAPC) as host to fabricate OLEDs.

In this host–guest system, the emissive materials are diluted in the host matrix, device efficiency and colour purity is enhanced *via* efficient Forster energy transfer. Compared to pristine thin film, it is evident that the doped film display hypochromatically shifted and narrow PL spectra showing improved PLQY of 0.82, 0.85, 0.89, 0.91, 0.93 and 0.95 for *m*-MTDATA:PPI-Cz or PPICN-Cz or PPI-An or PPICN-An or PPI-Py or PPICN-Py, respectively. Then, electroluminescent devices based on doped light-emitting layers with ITO/NPB (40 nm)/*m*-MTDATA:PPI-Cz or PPICN-Cz or PPI-An or PPICN-An or PPI-Py or PPICN-Py (20 nm)/TPBi (25 nm)/LiF (1 nm)/Al (100 nm) have been fabricated. The PL spectra of the doped devices (*m*-MTDATA:PPI-Cz or PPICN-Cz or PPI-Anor PPICN-An or PPI-Py or PPICN-Py) were similar to PL spectra of pure PPI-Cz or PPICN-Cz or PPI-An or PPICN-An or PPI-Py or PPICN-Py and did not contain bands at wavelength close to low energy band observed in EL spectra of doped OLEDs. The similarity of shape and position of PL spectra of the mixtures compared to PL spectra of pure emitters confirm energy transfer from host to emitters. The EL spectra of the doped devices are much more stable than the corresponding nondoped devices. Furthermore, blue-shifted EL emission was observed when compared to the corresponding nondoped devices especially for the OLEDs employing TPI-An or TPI-Py. Diluting the emitter molecules in the host eliminates the effect of intermolecular close stacking and decreased medium polarity because *m*-MTDATA is generally used as a nonpolar host material. The *m*-MTDATA:PPI-Cz/PPICN-Cz, *m*-MTDATA:PPI-An/PPICN-An and *m*-MTDATA:PPI-Py/PPICN-Py based OLEDs show improved device efficiencies (Fig. 7): η_{ex} (%) – 4.81/5.23, 5.01/5.25 and 5.61/5.76; η_c (cd A^{-1}) – 1.03/2.01, 4.90/5.00, 8.56/9.13: η_p (lm W^{-1}) – 1.00/1.38, 4.02/4.83 and 8.23/8.87, respectively. The doped device based on TAPC host TAPC:PPI-Cz/PPICN-Cz, PPI-An/PPICN-An and PPI-Py/PPICN-Py exhibit maximum efficiencies of η_c – 1.08/2.03, 4.93/5.02 and 8.58/9.15 cd A; η_p – 1.04/1.40, 4.04/4.85 and 8.26/8.90 lm W^{-1}; η_{ex} – 4.85/5.26, 5.04/5.28 and 5.65/5.78% (20 wt%). The doped OLEDs, *m*-MTDATA/TAPC:PPI-Cz (4.81/

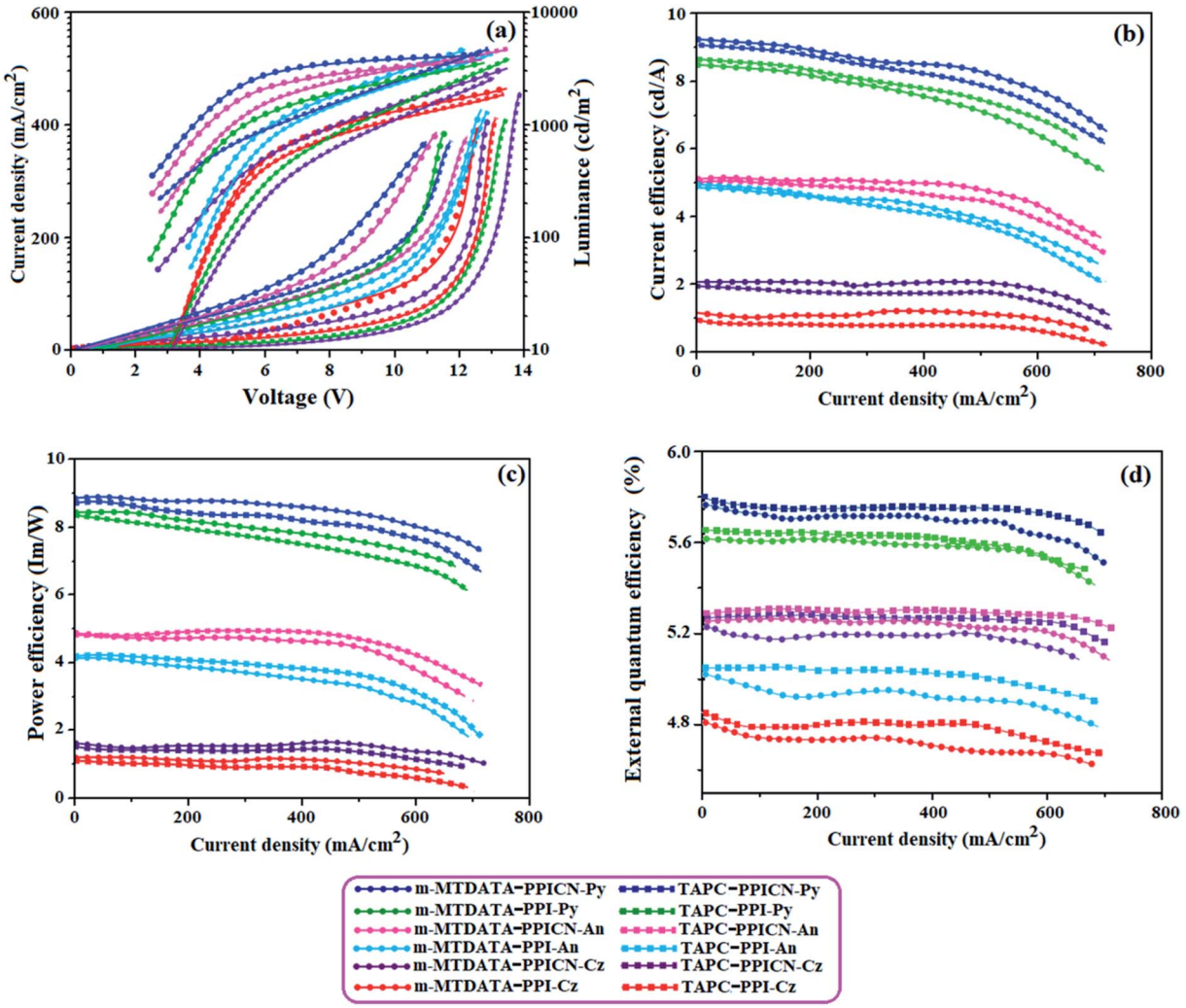

Fig. 7 Doped device efficiencies: (a) luminance/current density–voltage; (b) current efficiency–current density; (c) power efficiency–current density; (d) external quantum efficiency–current density of emissive materials.

Table 3 Electroluminescent performances of doped devices

Efficiency	*m*-MTDATA/ TAPC-PPI-Cz	*m*-MTDATA/ TAPC-PPICN-Cz	*m*-MTDATA/ TAPC-PPI-An	*m*-MTDATA/ TAPC-PPICN-An	*m*-MTDATA/ TAPC-PPI-Py	*m*-MTDATA/ TAPC -PPICN-Py
V_{on} (V)	3.1/3.0	3.0/2.8	3.7/3.6	2.8/2.6	3.0/2.6	2.8/2.5
η_c (cd A^{-1})	1.03/1.08	2.01/2.03	4.90/4.93	5.00/5.02	8.56/8.58	9.13/9.15
η_p (lm W^{-1})	1.00/1.04	1.38/1.40	4.02/4.04	4.83/4.85	8.23/8.26	8.87/8.90
η_{ex} (%)	4.81/4.85	5.23/5.26	5.01/5.04	5.25/5.28	5.61/5.65	5.76/5.78
EL (nm)	403, 540/402, 539	400, 538/400, 540	413, 539/414, 538	412, 536/410, 540	453, 540/450, 544	441, 539/436, 542
CIE (x,y)	0.15, 0.09	0.158, 0.08	0.15, 0.09	0.15, 0.08	0.15, 0.09	0.15, 0.08
L (cd m^{-2})	2036/2083	3183/3267	4146/4208	4252/4270	4201/4219	4703/4742

4.85%), *m*-MTDATA/TAPC:PPICN-Cz (5.23/5.26%), *m*-MTDATA/TAPC:PPI-An (5.01/5.04%), *m*-MTDATA/TAPC:PPICN-An (5.25/5.28%), *m*-MTDATA/TAPC:PPI-Py (5.61/5.65%) and *m*-MTDATA/TAPC:PPICN-Py (5.76/5.78) show improved efficiencies compared to that of nondoped devices, PPI-Cz (3.56%), PPICN-Cz (5.02%), PPI-An (4.08%), PPICN-An (5.10%), PPI-Py (5.56%) and PPICN-Py (5.80%). The V_{on} is raised from 2.4 to 3.7 V because of larger energy gap of the host (Table 3).

The electroluminescent efficiency is improved upon increasing the doping level (20 wt%) and these improved photometric efficiencies are partly ascribed to bathochromically shifted EL spectra in the heavily doped OLEDs. These improved performances are due to the absence of excimer emission by

using doping technique compared to TPI-Py based doped OLEDs with negligible excimer. It is observed that the current density in the heavily doped OLEDs increases faster than the devices with low dopant concentration. The doped devices with high performances show deep-blue emission in the series. The doped devices with PPI-Py and PPICN-Py show the best performances with deep-blue emission in the series. These experimental results reveal that non-doped and doped devices based on PPI-Cz, PPICN-Cz, PPI-An, PPICN-An, PPI-Py and PPICN-Py showing the accuracy for our molecular-design-strategy.

4. Conclusion

We have reported different aromatically substituted phenanthroimidazoles at C6 and C9 positions, PPI-Cz, PPICN-Cz, PPI-An, PPICN-An, PPI-Py and PPICN-Py for efficient OLEDs. The intramolecular charge transfer between N-phenylcarbazole/anthracene/pyrene fragments at C6/C9 positions and phenanthrimidazole core has been confirmed by experimental and theoretical studies. Photophysical studies reveal that C6 and C9 substituents induced moderate conjugation relative to C2 modification. Among the non-doped devices, pyrene substituted PPI-Py or PPICN-Py based devices show maximum efficiency: PPI-Py/PPICN-Py: η_c (cd A^{-1}) – 9.20/9.98; η_p (lm W^{-1}) – 8.50/9.16; η_{ex} (%) – 5.56/5.80. The doped OLEDs, *m*-MTDATA/TAPC:PPI-Cz (4.81/4.85%), *m*-MTDATA/TAPC:PPICN-Cz (5.23/5.26%), *m*-MTDATA/TAPC:PPI-An (5.01/5.04%), *m*-MTDATA/TAPC:PPICN-An (5.25/5.28%), *m*-MTDATA/TAPC:PPI-Py (5.61/5.65%) and *m*-MTDATA/TAPC:PPICN-Py (5.76/5.78%) show improved device efficiencies compared to that of nondoped devices. Designing C6/C9-modified phenanthrimidazole fluorophores is an efficient approach for constructing highly efficient OLEDs.

Conflicts of interest

There are no conflicts to declare.

References

1 Y. Im, S.-Y. Byun, J. H. Kim, D.-R. Lee, C. S. Oh, K.-S. Yook and J. Y. Lee, Recent progress in high-efficiency blue-light-emitting materials for organic light-emitting diodes, *Adv. Funct. Mater.*, 2017, **27**(13), 1603007–1603031.

2 Z. Wang, P. Lu, S. Chen, Z. Gao, F. Shen, W. Zhang, Y. Xu, H. S. Kwok and Y. Ma, Phenanthro[9,10-*d*]imidazole as a new building block for blue light emitting materials, *J. Mater. Chem.*, 2011, **21**(14), 5451–5457.

3 Z. Jiang, Z. Liu, C. Yang, C. Zhong, J. Qin, G. Yu and Y. Liu, Multifunctional fluorine based oligomers with novel spiro-annulated triarylamine: efficient, stable deep-blue electroluminescence, good hole injection, and transporting materials with very high tg, *Adv. Funct. Mater.*, 2009, **19**(24), 3987–3995.

4 H. H. Chou, Y. H. Chen, H.-P. Hsu, W. H. Chang, Y. H. Chen and C. H. Cheng, Synthesis of diimidazolylstilbenes as n-type blue fluorophores: alternative dopant materials for highly efficient electroluminescent devices, *Adv. Mater.*, 2012, **24**(43), 5867–5871.

5 H. Sasabe and J. Kido, Development of high performance OLEDs for general lighting, *J. Mater. Chem. C*, 2013, **1**(9), 1699–1707.

6 G. B. Bodedla, K. R. Justin Thomas, M. S. Fan and K. C. Ho, Benzimidazole-branched isomeric dyes: effect of molecular constitution on photophysical, electrochemical, and photovoltaic properties, *J. Org. Chem.*, 2016, **81**(2), 640–653.

7 S. W. Culligan, A. A. Chen, J. U. Wallace, K. P. Klubek, C. W. Tang and S. H. Chen, Effect of hole mobility through emissive layer on temporal stability of blue organic light-emitting diodes, *Adv. Funct. Mater.*, 2006, **16**(11), 1481–1488.

8 Y. Y. Lyu, J. Kwak, O. Kwon, S. H. Lee, D. Kim, C. Lee and K. Char, Silicon-cored anthracene derivatives as host materials for highly efficient blue organic light-emitting devices, *Adv. Mater.*, 2008, **20**(14), 2720–2729.

9 A. L. Fisher, K. E. Linton, K. T. Kamtekar, C. Pearson, M. R. Bryce and M.-C. Petty, Efficient deep-blue electroluminescence from an ambipolar fluorescent emitter in a single-active-layer device, *Chem. Mater.*, 2011, **23**(7), 1640–1642.

10 X. Tang, L. Yao, H. Liu, F. Shen, S. Zhang, Y. Zhang, H. Zhang, P. Lu and Y. Ma, Novel violet emitting material synthesized by stepwise chemical reactions, *J. Mater. Chem. C*, 2014, **2**(25), 5019–5046.

11 A.-P. Kulkarni, C. J. Tonzola, A. Babel and S. A. Jenekhe, Electron transport materials for organic light-emitting diodes, *Chem. Mater.*, 2004, **16**(23), 4556–4573.

12 Y. Shirota and H. Kageyama, Charge carrier transporting molecular materials and their applications in devices, *Chem. Rev.*, 2007, **107**(4), 953–1010.

13 A. Riaño, I. Arrechea-Marcos, M. J. Mancheño, P. Mayorga Burrezo, A. de la Peña, S. Loser, A. Timalsina, A. Facchetti, T. J. Marks, J. Casado, J. T. López Navarrete, R. Ponce Ortiz and J. L. Segura, Benzotrithiophene versus benzo/naphthodithiophene building blocks: the effect of star-shaped versus linear conjugation on their electronic structures, *Chem.–Eur. J.*, 2016, **22**(18), 6374–6381.

14 L. Chen, Y. Jiang, H. Nie, R. Hu, H. S. Kwok, F. Huang, A. Qin, Z. Zhao and B. Z. Tang, Rational design of aggregation-induced emission luminogen with weak electron donor–acceptor interaction to achieve highly efficient undoped bilayer OLEDs, *ACS Appl. Mater. Interfaces*, 2014, **6**(19), 17215–17225.

15 F. S. Melkonyan, W. Zhao, M. Drees, N. D. Eastham, M. J. Leonardi, M. R. Butler, Z. Chen, X. Yu, R. P. H. Chang, M. A. Ratner, A. F. Facchetti and T. J. Marks, Bithiophenesulfonamide building block for π-conjugated donor–acceptor semiconductors, *J. Am. Chem. Soc.*, 2016, **138**(22), 6944–6947.

16 W. C. Chen, Q. X. Tong and C.-S. Lee, The development of phenanthroimidazole derivatives in blue-emitting organic electroluminescence, *Sci. Adv. Mater.*, 2015, **7**(10), 2193–2205.

17 C. J. Kuo, T. Y. Li, C. C. Lien, C. H. Liu, F. I. Wu and M. J. Huang, Bis(phenanthroimidazolyl)biphenyl

derivatives as saturated blue emitters for electroluminescent devices, *J. Mater. Chem.*, 2009, **19**(18), 1865–1871.

18 Y. Zhang, S. L. Lai, Q. X. Tong, M. F. Lo, T. W. Ng, M. Y. Chan, Z. C. Wen, J. He, K. S. Jeff, X. L. Tang, W. M. Liu, C. C. Ko, P. F. Wang and C. S. Lee, High efficiency nondoped deep-blue organic light emitting devices based on imidazole-π-triphenylamine derivatives, *Chem. Mater.*, 2012, **24**(1), 61–70.

19 Y. T. Chang, S. L. Hsu, M. H. Su and K. H. Wei, Intramolecular donor–acceptor regioregular poly(hexylphenanthrenyl-imidazolethiophene) exhibits enhanced hole mobility for heterojunction solar cell applications, *Adv. Mater.*, 2009, **21**(20), 2093–2097.

20 Y. T. Chang, S. L. Hsu, G. Y. Chen, M. H. Su, T. A. Singh, E. W. G. Diau and K. H. Wei, Intramolecular donor–acceptor regioregular poly(3-hexylthiophene)s presenting octylphenanthrenyl-imidazole moieties exhibit enhanced charge transfer for heterojunction solar cell applications, *Adv. Funct. Mater.*, 2008, **18**(16), 2356–2365.

21 H. C. Wu, A. D. Yu, W.-Y. Lee, C. L. Liu and W. C. Chen, A poly(fluorene-thiophene) donor with a tethered phenanthro[9,10-*d*]imidazole acceptor for flexible nonvolatile flash resistive memory devices, *Chem. Commun.*, 2012, **48**(73), 9135–9137.

22 M. S. Subeesh, K. Shanmugasundaram, C. D. Sunesh, Y. S. Won and Y. Choe, Utilization of a phenanthroimidazole based fluorophore in light-emitting electrochemical cells, *J. Mater. Chem. C*, 2015, **3**(18), 4683–4687.

23 L. K. Zhang, G. F. Wu, Y. Zhang, Y. C. Tian, Q. X. Tong and D. Li, A two-in-one fluorescent sensor with dual channels to detect Zn^{2+} and Cd^{2+}, *RSC Adv.*, 2013, **3**(44), 21409–21412.

24 C. H. Tseng, C. C. Tzeng, P. K. Shih, C. N. Yang, Y. C. Chuang, S. I. Peng, C. S. Lin, J. P. Wang, C. M. Cheng and Y. L. Chen, Identification of furo[3,2:3,4]naphtho[1,2-*d*]imidazole derivatives as orally active and selective inhibitors of microsomal prostaglandine 2 synthase-1 (mpges-1), *Mol. Diversity*, 2012, **16**(2), 215–229.

25 R. Francke and R.-D. Little, Optimizing electron transfer mediators based on arylimidazoles by ring fusion: synthesis, electrochemistry, and computational analysis of 2-aryl-1-methylphenanthro[9,10-*d*]imidazoles, *J. Am. Chem. Soc.*, 2014, **136**(1), 427–435.

26 B. Liu, J. Zhao, C. Luo, F. Lu, S. Tao and Q. Tong, A novel bipolar phenanthroimidazole derivative host material for highly efficient green and orange-red phosphorescent OLEDs with low efficiency roll-off at high brightness, *J. Mater. Chem. C*, 2016, **4**(10), 2003–2013.

27 W. C. Chen, Y. Yuan, S. F. Ni, Z. L. Zhu, J. Zhang, Z. Q. Jiang, L. S. Liao, F. L. Wong and C. S. Lee, Highly efficient deep-blue electroluminescence from a charge-transfer emitter with stable donor skeleton, *ACS Appl. Mater. Interfaces*, 2017, **9**(8), 7331–7338.

28 Y. Yuan, J. X. Chen, F. Lu, Q. X. Tong, Q. D. Yang, H. W. Mo, T. W. Ng, F. L. Wong, Z. Q. Guo, J. Ye, Z. Chen, X. H. Zhang and C. S. Lee, Bipolar phenanthroimidazole derivatives containing bulky polyaromatic hydrocarbons for nondoped blue electroluminescence devices with high efficiency and low efficiency roll-off, *Chem. Mater.*, 2013, **25**(24), 4957–4965.

29 Y. Zhang, J.-H. Wang, G. Han, F. Lu and Q.-X. Tong, Phenanthroimidazole derivatives as emitters for non-doped deep- blue organic light emitting devices, *RSC Adv.*, 2016, **6**(75), 70800–70809.

30 Z. Wang, Y. Feng, S. Zhang, Y. Gao, Z. Gao, Y. Chen, X. Zhang, P. Lu, B. Yang, P. Chen, Y. Ma and S. Liu, Construction of high efficiency non-doped deep blue emitters based on phenanthroimidazole: remarkable substitution effects on the excited state properties and device performance, *Phys. Chem. Chem. Phys.*, 2014, **16**(38), 20772–20781.

31 C. J. Kuo, T. Y. Li, C. C. Lien, C. H. Liu, F. I. Wu and M. J. Huang, Bis(phenanthroimidazolyl)biphenyl derivatives as saturated blue emitters for electroluminescent devices, *J. Mater. Chem.*, 2009, **19**(13), 1865–1936.

32 S. Zhang, L. Yao, Q. Peng, W. Li, Y. Pan, R. Xiao, Y. Gao, C. Gu, Z. Wang, P. Lu, F. Li, S. Su, B. Yang and Y. Ma, Achieving a significantly increased efficiency in nondoped pure blue fluorescent OLED: a quasi-equivalent hybridized excited state, *Adv. Funct. Mater.*, 2015, **25**, 1755–1762.

33 S. K. Kim, B. Yang, Y. Ma, J. H. Lee and J. W. Park, Exceedingly efficient deep-blue electroluminescence from new anthracenes obtained using rational molecular design, *J. Mater. Chem.*, 2008, **18**, 3376–3384.

34 (*a*) M. J. Frisch, G. W. Trucks, H. B. Schlegel, G. E. Scuseria, M. A. Robb, J.-R. Cheeseman, J. A. Montgomery, T. Vreven, K.-N. Kudin, J.-C. Burant, J. M. Millam, S. S. Iyengar, J. Tomasi, V. Barone, B. Mennucci, M. Cossi, G. Scalmani, N. Rega, G. A. Petersson, H. Nakatsuji, M. Hada, M. Ehara, K. Toyota, R. Fukuda, J. Hasegawa, M. Ishida, T. Nakajima, Y. Honda, O. Kitao, H. Nakai, M. Klene, X. Li, J. E. Knox, H. P. Hratchian, J. B. Cross, V. Bakken, C. Adamo, J. Jaramillo, R. Gomperts, R. E. Stratmann, O. Yazyev, A. J. Austin, R. Cammi, C. Pomelli, J. W. Ochterski, P. Y. Ayala, K. Morokuma, G. A. Voth, P. Salvador, J. J. Dannenberg, V. G. Zakrzewski, S. Dapprich, A. D. Daniels, M. C. Strain, O. Farkas, D. K. Malick, A. D. Rabuck, K. Raghavachari, J. B. Foresman, J. V. Ortiz, Q. Cui, A.-G. Baboul, S. Clifford, J. Cioslowski, B.-B. Stefanov, G. Liu, A. Liashenko, P. Piskorz, I. Komaromi, R. L. Martin, D. J. Fox, T. Keith, M. A. A. Laham, C. Y. Peng, A. Nanayakkara, M. Challacombe, P. M. W. Gill, B. Johnson, W. Chen, M. W. Wong, C. Gonzalez and J. A. Pople, *Gaussian 09 (Revision A.02)*, Gaussian, Inc., Wallingford, CT, 2009; (*b*) T. Lu and F. Chen, *J. Comput. Chem.*, 2012, **33**, 580–592.

35 J. Jayabharathi, G. Goperundevi and S. Panimozhi, Regulation of singlet and triplet excitons in a single emission layer: efficient fluorescent/phosphorescent hybrid white organic light-emitting diodes, *ACS Omega*, 2019, **4**, 15030–15042.

36 S. Zhang, L. Yao, Q. Peng, W. Li, Y. Pan, R. Xiao, Y. Gao, C. Gu, Z. Wang, P. Lu, F. Li, S. Su, B. Yang and Y. Ma, Achieving a significantly increased efficiency in nondoped

pure blue fluorescent OLED: a quasi-equivalent hybridized excited state, *Adv. Funct. Mater.*, 2015, **25**, 1755–1762.

37 J. Jayabharathi, S. Panimozhi and V. Thanikachalam, Asymmetrically twisted phenanthroimidazole derivatives as host materials for blue fluorescent, green and red phosphorescent OLEDs, *Sci. Rep.*, 2019, **9**, 1–14.

38 G.-B. Bodedla, K. R. Justin Thomas, M.-S. Fan and K. C. Ho, Benzimidazole-branched isomeric dyes: effect of molecular constitution on photophysical, electrochemical, and photovoltaic properties, *J. Org. Chem.*, 2016, **81**, 640–653.

39 W. C. Chen, Y. Yuan, Y. Xiong, A. L. Rogach, Q. X. Tong and C. S. Lee, Aromatically C6- and C9-substituted phenanthro [9,10-*d*]imidazole blue fluorophores: structure–property relationship and electroluminescent application, *ACS Appl. Mater. Interfaces*, 2017, **9**, 26268–26278.

40 W. C. Chen, Q. X. Tong and C. S. Lee, The development of phenanthroimidazole derivatives in blue-emitting organic electroluminescence, *Sci. Adv. Mater.*, 2015, **7**(10), 2193–2205.

41 Y. Zhang, S. L. Lai, Q. X. Tong, M. F. Lo, T. W. Ng, M. Y. Chan, Z. C. Wen, J. He, K. S. Jeff, X. L. Tang, W. M. Liu, C. C. Ko, P. F. Wang and C. S. Lee, High efficiency non-doped deep-blue organic light emitting devices based on imidazole-*p*-triphenylamine derivatives, *Chem. Mater.*, 2011, **24**(1), 61–70.

42 W. C. Chen, Y. Yuan, G. F. Wu, H. X. Wei, L. Tang, Q. X. Tong, F. L. Wong and C. S. Lee, Staggered face-to-face molecular stacking as a strategy for designing deep-blue electroluminescent materials with high carrier mobility, *Adv. Opt. Mater.*, 2014, **2**(7), 626–631.

43 C. Li, S. Wang, W. Chen, J. Wei, G. Yang, K. Ye, Y. Liu and Y. Wang, High performance full color OLEDs based on a class of molecules with dual carrier transport channels and small singlet triplet splitting, *Chem. Commun.*, 2015, **51**(53), 10632–10635.

44 H. Huang, Y. Wang, B. Wang, S. Zhuang, B. Pan, X. Yang, L. Wang and C. Yang, Controllably tunable phenanthroimidazole carbazole hybrid bipolar host materials for efficient green electrophosphorescent devices, *J. Mater. Chem. C*, 2013, **1**(37), 5899–5908.

45 Z. Gao, Z. Wang, T. Shan, Y. Liu, F. Shen, Y. Pan, H. Zhang, X. He, P. Lu, B. Yang and Y. Ma, High-efficiency deep blue fluorescent emitters based on phenanthro[9,10-*d*]imidazole substituted carbazole and their applications in organic light emitting diodes, *Org. Electron.*, 2014, **15**(11), 2667–2676.

46 Y. Zhang, T.-W. Ng, F. Lu, Q.-X. Tong, S.-L. Lai, M. Y. Chan, H.-L. Kwong and C.-S. Lee, A pyrene-phenanthroimidazole derivative for non-doped blue organic light-emitting devices, *Dyes Pigm.*, 2013, **98**(2), 190–194.

47 (*a*) Z.-R. Grabowski, K. Rotkiewicz and W. Rettig, Structural changes accompanying intramolecular electron transfer: focus on twisted intramolecular charge-transfer states and structures, *Chem. Rev.*, 2003, **103**(10), 3899–4032; (*b*) J. Jayabharathi, J. Anudeebhana, V. Thanikachalam, S. Sivaraj and A. Prabhakaran, Efficient donor–acceptor emitter based nonsymmetrical connection for organic emitting diodes with improving exciton utilization, *RSC Adv.*, 2020, **10**(7), 4002–4013.

48 E. Lippert, Spectroscopic determination of the dipole moment of aromatic compounds in the first excited singlet state, *Z. Elektrochem.*, 1957, **61**(8), 962–975.

49 N. Mataga, Y. Kaifu and M. Koizumi, Solvent effects upon fluorescence spectra and the dipole moments of excited molecules, *Bull. Chem. Soc. Jpn.*, 1956, **29**(4), 465–470.

50 S. Zhang, W. Li, L. Yao, Y. Pan, F. Shen, R. Xiao, B. Yang and Y. Ma, Enhanced proportion of radiative excitons in non-doped electro-fluorescence generated from an imidazole derivative with an orthogonal donor–acceptor structure, *Chem. Commun.*, 2013, **49**(96), 11302–11304.

51 W. Li, Y. Pan, R. Xiao, Q. Peng, S. Zhang, D. Ma, F. Li, F. Shen, Y. Wang, B. Yang and Y. Ma, Employing – 100% excitons in oleds by utilizing a fluorescent molecule with hybridized local and charge-transfer excited state, *Adv. Funct. Mater.*, 2014, **24**(11), 1609–1614.

52 S. Zhang, L. Yao, Q. Peng, W. Li, Y. Pan, R. Xiao, Y. Gao, C. Gu, Z. Wang, P. Lu, F. Li, S. Su, B. Yang and Y. Ma, Achieving a significantly increased efficiency in non-doped pure blue fluorescent OLED: a quasi-equivalent hybridized excited state, *Adv. Funct. Mater.*, 2015, **25**(11), 1755–1762.

53 Y. Yuan, D. Li, X. Zhang, X. Zhao, Y. Liu, J. Zhang and Y. Wang, Phenanthroimidazole-derivative semiconductors as functional layer in high performance OLEDs, *New J. Chem.*, 2011, **35**(7), 1534–1540.

54 Y. Liu, L.-S. Cui, M.-F. Xu, X.-B. Shi, D.-Y. Zhou, Z.-K. Wang, Z.-Q. Jiang and L.-S. Liao, Highly efficient single-layer organic light-emitting devices based on a bipolar pyrazine/carbazole hybrid host material, *J. Mater. Chem. C*, 2014, **2**(14), 2488–2495.

55 Y.-H. Lou, M.-F. Xu, L. Zhang, Z.-K. Wang, S. Naka, H. Okada and L.-S. Liao, Origin of enhanced electrical and conducting properties in pentacene films doped by molybdenum trioxide, *Org. Electron.*, 2013, **14**(10), 2698–2704.

56 Z. Wang, Y. Lou, S. Naka and H. Okada, Bias and temperature dependent charge transport in solution-processed small molecular mixed single layer organic light emitting devices, *Appl. Phys. Lett.*, 2011, **98**(6), 063302–063306.

57 M. J. Cho, S. J. Kim, S. H. Yoon, J. Shin, T. R. Hong and H. J. Kim, New bipolar host materials for realizing blue phosphorescent organic light-emitting diodes with high efficiency at 1000 cd m^{-2}, *ACS Appl. Mater. Interfaces*, 2014, **6**(22), 19808–19815.

58 H. Wang, L. Meng, X. Shen, X. Wei, X. Zheng, X. Lv, Y. Yi, Y. Wang and P. Wang, Highly efficient orange and red phosphorescent organic light-emitting diodes with low roll-off of efficiency using a novel thermally activated delayed fluorescence material as host, *Adv. Mater.*, 2015, **27**(27), 4041–4047.

59 V. Bulovic, V.-B. Khalfin, G. Gu, P.-E. Burrows, D.-Z. Garbuzov and S.-R. Forrest, Weak microcavity effects in organic light-emitting devices, *Phys. Rev. B: Condens. Matter Mater. Phys.*, 1998, **58**(7), 3730–3740.

60 W.-C. Chen, Y. Yuan, G. F. Wu, H. X. Wei, J. Ye, M. Chen, F. Lu, Q. X. Tong, F. L. Wong and C. S. Lee, Molecular modification on bisphenanthroimidazole derivative for deep-blue organic electroluminescent material with ambipolar property and high performance, *Org. Electron.*, 2015, **17**, 159–166.

61 W. C. Chen, Y. Yuan, S. F. Ni, Q. X. Tong, F. L. Wong and C. S. Lee, Achieving efficient violet-blue electroluminescence with CIE*y* < 0.06 and EQE > 6% from naphthyl-linked phenanthroimidazole–carbazole hybrid fluorophores, *Chem. Sci.*, 2017, **8**(5), 3599–3608.

62 X. Tang, Q. Bai, Q. Peng, Y. Gao, J. Li, Y. Liu, L. Yao, P. Lu, B. Yang and Y. Ma, Efficient deep blue electroluminescence with an external quantum efficiency of 6.8% and CIE*y* < 0.08 based on a phenanthroimidazole–sulfone hybrid donor–acceptor molecule, *Chem. Mater.*, 2015, **27**(20), 7050–7057.

63 I. Kondrasenko, Z. H. Tsai, K. Chung, Y. T. Chen, Y. Y. Ershova, A. Doménech-Carbó, W. Y. Hung, P. T. Chou, A. J. Karttunen and I. O. Koshevoy, Ambipolar phosphine derivatives to attain true blue OLEDs with 6.5% EQE, *ACS Appl. Mater. Interfaces*, 2016, **8**(17), 10968–10976.

64 A. Obolda, Q. Peng, C. He, T. Zhang, J. Ren, H. Ma, Z. Shuai and F. Li, Triplet-polaron–interaction-induced up conversion from triplet to singlet: a possible way to obtain highly efficient OLEDs, *Adv. Mater.*, 2016, **28**(23), 4740–4746.

